

# Low-lying Proton Intruder State in $^{13}\text{B}$

S. Ota<sup>a</sup> S. Shimoura<sup>a</sup> H. Iwasaki<sup>b</sup> M. Kurokawa<sup>c</sup>

S. Michimasa<sup>a</sup> N. Aoi<sup>c</sup> H. Baba<sup>c</sup> K. Demichi<sup>d</sup> Z. Elekes<sup>e</sup>

T. Fukuchi<sup>c</sup> T. Gomi<sup>c</sup> S. Kanno<sup>c</sup> S. Kubono<sup>a</sup> K. Kurita<sup>d</sup>

H. Hasegawa<sup>d</sup> E. Ideguchi<sup>a</sup> N. Iwasa<sup>f</sup> Y.U. Matsuyama<sup>d</sup>

K.L. Yurkewicz<sup>g</sup> T. Minemura<sup>c</sup> T. Motobayashi<sup>c</sup>

T. Murakami<sup>h</sup> M. Notani<sup>i</sup> A. Odahara<sup>j</sup> A. Saito<sup>b</sup> H. Sakurai<sup>c</sup>

E. Takeshita<sup>c</sup> S. Takeuchi<sup>c</sup> M. Tamaki<sup>a</sup> T. Teranishi<sup>k</sup>

Y. Yanagisawa<sup>c</sup> K. Yamada<sup>c</sup> M. Ishihara<sup>c</sup>

<sup>a</sup>*Center for Nuclear Study, University of Tokyo, Saitama 351-0198, Japan*

<sup>b</sup>*Department of Physics, University of Tokyo, Tokyo 113-0033, Japan*

<sup>c</sup>*RIKEN Nishina Center for Accelerator-Based Science, Saitama 351-0198, Japan*

<sup>d</sup>*Department of Physics, Rikkyo University, Tokyo 171-8501, Japan*

<sup>e</sup>*Hungarian Acad. Sci., Inst. Nucl. Res., H-4001 Debrecen, Hungary*

<sup>f</sup>*Department of Physics, Tohoku University, Miyagi 980-8578, Japan*

<sup>g</sup>*NSCL, Michigan State University, East Lansing, MI 48824, USA*

<sup>h</sup>*Department of Physics, Kyoto University, Kyoto 606-8502, Japan*

<sup>i</sup>*Argonne National Laboratory, Argonne, IL 60439, USA*

<sup>j</sup>*Department of Physics, Osaka University 560-0043, Japan*

<sup>k</sup>*Department of Physics, Kyushu University, 812-8581*

## Abstract

The neutron rich nucleus  $^{13}\text{B}$  was studied via the proton transfer reaction  $^4\text{He}(^{12}\text{Be},^{13}\text{B}\gamma)$  at 50A MeV. The known 4.83-MeV excited state was strongly populated and its spin and parity were assigned to  $1/2^+$  by comparing the angular differential cross section data with DWBA calculations. This low-lying  $1/2^+$  state is interpreted as a proton intruder state and indicates a deformation of the nucleus.

*Key words:* Intruder state, Proton single particle state, Proton transfer reaction,  $^4\text{He}(^{12}\text{Be},^{13}\text{B}\gamma)$ ,

*PACS:* 21.10.Pc, 25.55.Hp, 27.20.+n, 29.30.Kv

---

The existence of intruder states in light neutron-rich unstable nuclei is often considered to be evidence for one or more  $\hbar\omega$  configurations in the low-lying states around the *psd* shell. The ground state of  $^{11}\text{Be}$  is  $1/2^+$  which is lower in energy by 0.3 MeV than the  $1/2^-$  state [1]. In  $^{12}\text{Be}$ , there is a  $1^-$  intruder state at 2.7-MeV excitation energy [2]. The energies of these low-lying, non-normal parity states indicate  $1\hbar\omega$  configurations. Furthermore, the presence of low-lying  $2_1^+$  [3] and  $0_2^+$  [4,5] states in  $^{12}\text{Be}$  suggests a  $2\hbar\omega$  configuration.

Three theoretical interpretations have been proposed for these one or more  $\hbar\omega$  configurations in the low-lying states of neutron-rich unstable nuclei: (1) the monopole interaction of the tensor force [6], (2) the loosely bound nature of some orbitals [7], and (3) nuclear deformation [5,8,9]. In Ref. [6], the effective interaction was determined so that the model reproduces the energy levels in light, neutron-rich nuclei including intruder states, and the importance of monopole interaction due to the tensor force was pointed out. Reference [7] discusses the fact that in the *psd* shell, the  $2s_{1/2}$  orbital gains its energy relative to the other orbitals due to its loosely bound nature. The non-zero

$\hbar\omega$  configurations can also be intuitively explained by the deformed mean field picture. As seen in the Nilsson diagram, the gap becomes smaller with increasing deformation [5,8,9]. Since the combination of these effects, which are provided by their corresponding theoretical models, changes the neutron shell structure in neutron-rich nuclei, such as  $^{11,12}\text{Be}$ , the relative importance of the three theoretical approaches has not been clarified.

For the proton shell in light neutron-rich nuclei, the effects due to the tensor force and the loosely bound nature of the orbitals are expected to be small since the  $\nu p_{1/2,3/2}$  orbitals are fully filled and the proton(s) are deeply bound. However, deformation is still presumed to affect the proton shell structure. Proton intruder states are, therefore, signatures for the importance of deformation. In the present study, we focus on the proton shell structure in the  $N = 8$  nucleus  $^{13}\text{B}$  by investigating the proton single-particle states.

In order to investigate the proton single-particle states in  $^{13}\text{B}$ , we used the  $(\alpha, t)$  reaction on  $^{12}\text{Be}$  in inverse kinematics. This process at an intermediate energy has a relatively large cross section since the proton to be transferred is deeply bound in the  $\alpha$  particle and, thus, has high-momentum components, which reduce the effect of the momentum mismatch of the  $(\alpha, t)$  reaction [10].

The experiment was performed at the RIKEN Accelerator Research Facility. A  $^{12}\text{Be}$  beam was produced by the fragmentation reaction of a 100A MeV  $^{18}\text{O}$  beam on a  $^9\text{Be}$  target with a thickness of 1.85-g/cm<sup>2</sup>. The  $^{12}\text{Be}$  beam was separated by the RIKEN Projectile-fragment Separator (RIPS) [12]. The incident particles were identified on an event-by-event basis using the measured time-of-flight and the energy deposited. The time-of-flight, over a path length of 5.4 m, and the energy deposited were measured using two plastic scintillators

located at the last two foci of the RIPS. The intensity and the purity of the  $^{12}\text{Be}$  beam respectively were typically  $2 \times 10^5$  counts per second and 90%.

The 50A MeV  $^{12}\text{Be}$  beam bombarded a secondary target of liquid helium[11] located at the final focus of the RIPS. A liquid helium target was chosen because of its statistical advantage in terms of the experimental yields. The helium was condensed by a cryogenic refrigerator and kept below 4 K during the experiment. A target thickness of  $143 \pm 5$  mg/cm<sup>2</sup> was estimated from the velocity difference between outgoing particles measured with and without the liquid helium. The positions and directions of the incident particles on the secondary target were deduced from the position information of two parallel plate avalanche counters [13] located 30-cm apart from each other around the final focus. The outgoing particles were detected by a plastic scintillator hodoscope 3.5-m downstream from the secondary target with a  $1 \times 1$  m<sup>2</sup> active area and an angular acceptance of up to 8 degrees in the laboratory frame. The plastic scintillator hodoscope consisted of 5-mm thick  $\Delta E$  and 60-mm thick  $E$  layers. The  $\Delta E$  layer was divided into 13 plastic scintillator bars vertically and the  $E$  layer into 16 plastic scintillator bars horizontally. The outgoing particles were identified on an event-by-event basis using the measured time-of-flight and the energy deposited in the  $\Delta E$  and  $E$  layers. The mass distribution for the  $Z = 5$  particles is shown in Fig. 1; the mass resolution ( $\delta A$ ) was determined to be  $\sim 0.25$ . The time-of-flight between the secondary target and the hodoscope was deduced from the time information of the plastic scintillators located upstream from the secondary target and the plastic scintillator hodoscope. Position information for the outgoing particles was deduced from the time difference between the output signals from the two photomultiplier tubes attached to both ends of each scintillator bar, and was

used to determine the scattering angle. The angular resolution of the scattering angle in the laboratory frame was 0.5 degrees in one standard deviation.

The de-excitation  $\gamma$  rays were detected by an array of germanium detectors: Gamma-Ray detector Array with Position and Energy sensitivities (GRAPE)[14]. This consisted of 6 germanium detectors located at  $140^\circ$  with respect to the beam axis. Each detector contains two cylindrical crystals 6 cm in diameter and 2 cm thick, with a common anode between them. The each cathode attached to each crystal is segmented into a  $3 \times 3$  matrix. The GRAPE provides position information of the  $\gamma$ -ray interaction point, which is extracted from a pulse shape analysis of the signal from the cathode [14,15]. The intrinsic energy resolution and the full energy peak efficiency were typically 2.7 keV (FWHM) and 0.4%, respectively, for 1332-keV  $\gamma$  rays from a  $^{60}\text{Co}$  standard source. The energy resolution after correcting for the Doppler shift was deduced to be 1.3% (FWHM) for 2.1-MeV  $\gamma$  rays, corresponding to the decay of the first  $2^+$  state of  $^{12}\text{Be}$  moving with 30% the light velocity. The excited states of  $^{13}\text{B}$  populated in the reaction were identified by measuring the energy of the de-excitation  $\gamma$  rays.

Figure 2 shows the energy spectrum of  $\gamma$  rays measured in coincidence with  $^{13}\text{B}$  after correcting for the Doppler shift. There are three peaks corresponding to the transitions from (3.68-, 3.73-), 4.13- and 4.83-MeV excited states to the ground state. The peaks seen in the low energy region is considered to originate from the reaction of the beam and the window of the target cell. Other significant transitions including those between the excited states were not observed in the present measurement. In the figure, hatched areas show the response functions of the GRAPE for the de-excitation  $\gamma$  rays obtained by means of a Monte Carlo simulation using the GEANT4 code [16,17] and

for the background  $\gamma$  rays. The background was assumed to consist of two components, the natural background  $\gamma$  rays, estimated by putting the gate in the non-prompt region of the time spectrum of the GRAPE, and the  $\gamma$  rays from the isomer state of  $^{12}\text{Be}$ , which were simulated by assuming a life time of 331 ns [5]. The ratio of the isomer state to the ground state in the secondary beam was less than 2 percent at the secondary target. In the simulations, all the resolutions of the detectors associated with the correction for the Doppler shift were taken into account. The intensity of each decay to the ground state was deduced by fitting the experimental spectrum with the sum of the response functions and the background. Assuming no cascade decay, the derived relative intensities of the observed  $\gamma$  rays from the known excited states are shown in Table 1, together with the previously reported data including two neutron transfer [18], neutron knockout [19],  $\beta$ -decay followed by neutron decay [20], and multi-nucleon transfer [21]. In the present reaction, the excited state at 4.83 MeV is strongly populated relative to the other excited states, while it is less excited in the other reactions except for the multi-nucleon transfer reaction which is expected to populate proton excited states. Considering the selectivity of the proton transfer reaction, it is conceivable that the 4.83-MeV excited state is of proton single-particle nature.

In order to determine the angular differential cross section of the  $^4\text{He}(^{12}\text{Be},^{13}\text{B}^*)$  reaction, individual  $\gamma$ -ray spectra with 0.5-degree-scattering-angle cuts were fitted with the same response functions and background described above, and they were analyzed to deduce the populations. Figure 3 shows the experimental angular distribution for the 4.83-MeV excitation with filled circles. The transferred angular momentum ( $\Delta L$ ) in the reaction is determined by comparing the obtained angular distributions with predictions of the distorted-wave Born

approximations (DWBA), calculated with the DWUCK5 code [22]. The optical potentials for the entrance and exit channels were obtained by adopting a single folding model used in Ref. [23]. The density distribution of  $^{12}\text{Be}$  for the folding is calculated by using the mean field calculation code, TIMORA[24,25]. The density distribution of  $^{13}\text{B}$  is assumed to be the same as that of  $^{12}\text{Be}$  with  $R(^{13}\text{B})/R(^{12}\text{Be}) = (13/12)^{1/3}$ . For the entrance channel, the depth of the imaginary potential is adjusted so as to represent the inelastic scattering data of  $^{12}\text{Be}$ , excited to the  $2_1^+$  state. For the exit channel, the depths of the real and imaginary potentials are varied in order to estimate the statistical error for the spectroscopic factor. The DWBA predictions with  $\Delta L = 0, 1, 2$  are shown as curves in Fig. 3. The absolute magnitudes of the predictions are normalized so as to minimize the  $\chi^2$  values. The reduced  $\chi^2$  value is 0.74 for the  $L = 0$  calculation. The forward angle peak in the experimental angular distribution is well described by the  $\Delta L = 0$  DWBA calculation. Therefore, we assigned a spin and parity of  $1/2^+$  to the 4.83-MeV excited state. Its low energy indicates that it is a proton intruder state from the  $sd$  shell. The spectroscopic strength  $C^2S$  was deduced to be  $0.20 \pm 0.02$ , where  $S$  is a spectroscopic factor and  $C^2$  is an isospin Clebsch-Gordan coefficient. The systematic errors of the  $C^2S$  due to the choice of the optical potentials in the DWBA calculation and to the geometrical uncertainty of the GRAPE in the simulation were evaluated to be 50% and 10%, respectively. The former one is obtained from the difference between the folding model and a separate calculation using a global optical potential for  $^{12}\text{C}$  in Ref. [26,27]. In the absolute magnitude of the differential cross section, there is no ambiguity originated from cascade decays to or from the 4.83-MeV excited state. No excited state was found above 4.83 MeV up to the neutron threshold of 4.87 MeV in  $^{13}\text{B}$ , therefore, the cascade decays to the 4.83-MeV excited state are unlikely to occur. On the other hand, the cascade

decay from the 4.83-MeV excited state is also small as explained below. The excited state ( $1/2^+$ ) is expected to decay to the ground state ( $3/2^-$ ) via an  $E1$  transition, whose decay rate is proportional to the cube of the transition energy, *i.e.*,  $E_\gamma^3$  [8]. The maximum possible transition energy to a known excited state is 1.4 MeV corresponding to the decay to the 3.48-MeV excited state. Even if the decay to this state is by  $E1$  transition, its decay rate is about 40 times smaller than to the ground state. Decay rates other than  $E1$  are also expected to be much smaller. In fact, no cascade decay of the 4.83-MeV excited state was observed in the present and the previous experiments.

There are few theoretical predictions for  $^{13}\text{B}$ . In Ref. [19], the result of a shell model calculation for  $^{13}\text{B}$  has been shown, however, the calculation is performed from the viewpoint of the neutron structure. Focusing on the proton shell structure, we performed a shell model calculation for  $^{13}\text{B}(^{12}\text{Be})$  with the calculation code, OXBASH [28], wherein the interaction including the effect of the tensor force and reproducing intruder states in the neutron-rich nuclei such as  $^{11,12}\text{Be}$  [6], is used. The model space consisting of the *psd* shell with maximum  $3(2)\hbar\omega$  excitation was considered for  $^{13}\text{B}(^{12}\text{Be})$ . The spectroscopic factor was calculated as the overlap between each excited state of  $^{13}\text{B}$  and the ground state of  $^{12}\text{Be}$ . The shell model calculation predicts four  $1/2^+$  states below 10 MeV excitation energy. Three lower states are predicted at 3.7, 6.5 and 9.1 MeV with spectroscopic strengths of 0.01, 0.03 and 0.003, respectively. These strengths are too small to explain the experimental result. The fourth  $1/2^+$  state with a spectroscopic strength of 0.30 is close to the experimental spectroscopic strength; however its excitation energy is 9.5 MeV. These results of the shell model calculation may indicate that the theoretical approach based on the effect of the tensor force does not explain the experimental result, or



the model space consisting of the  $psd$  shell and the excitation of  $3\hbar\omega$  are not large enough.

A simple expression for the observed  $1/2^+$  state with proton single particle nature is  $(\pi sd)^1 \otimes {}^{12}\text{Be}$ . Concerning the possible large deformation of  ${}^{12}\text{Be}$ , we examine the qualitative consequence of a deformed core. The  $1/2^+$  state arises with a configuration of  $(\pi[220\frac{1}{2}])^1$  to the  ${}^{12}\text{Be}(\text{g.s.})$  core. As seen in the Nilsson diagram, at large deformation, the  $\pi[220\frac{1}{2}]$  orbital gains energy. The energy gain of the total system compared to the spherical  $s_{1/2}$  is estimated to be around 7 MeV from the diagram and the semi-empirical mass formula with a deformation parameter of 0.5. The discrepancy between the shell model prediction mentioned above and the present result for the  $1/2^+$  state is thus ascribed to a core deformation effect. In the present reaction, the observed  $1/2^+$  state is considered to be populated by the transfer of a proton to the  $\pi[220\frac{1}{2}]$  orbital. Hence, the low excitation energy of the  $1/2^+$  state suggests a deformed mean field. Since the proton is transferred to the  $[220\frac{1}{2}]$  orbital by an  $s$ -wave ( $\Delta L = 0$ ), the spectroscopic factor of the spherical  $2s_{1/2}$  component in the  $[220\frac{1}{2}]$  orbital, *e.g.*  $S = 0.273$  at  $\delta = 0.4$  [8], may also reproduce the experimental result.

Based on the discussion above, the  $1/2^+$  intruder state at 4.83 MeV is a signature of a deformed field and indicates the importance of a deformation in this nuclei. On the other hand, the ground state of  ${}^{13}\text{B}$  is supposed to be spherical with a normal  $p$ -shell configuration [29]. The excitation of only one proton thus changes the structure of the nucleus.

Recently an AMD calculation related to the experimentally assigned  $1/2^+$  state of  ${}^{13}\text{B}$  was carried out by Kanada-En'yo et al [30]. The calculation pre-

dicts a largely deformed  $1/2_1^+$  state with proton  $1\hbar\omega$  excitation and neutron  $2\hbar\omega$  excitation. In the excited state, the last proton occupies a molecular  $\sigma$  orbital which has a density distribution similar to the  $[220\frac{1}{2}]$  Nilsson orbital. The  $1/2_1^+$  state predicted by AMD may correspond to the experimental one although the calculated excitation energy is 8 MeV.

In summary, we have studied the proton transfer reaction on  $^{12}\text{Be}$  in inverse kinematics. A spin and parity of  $1/2^+$  for the 4.83-MeV excited state in  $^{13}\text{B}$  were assigned for the first time. A spectroscopic strength of  $0.20 \pm 0.02$  was also obtained with 60% systematic error. This state is interpreted to be a proton intruder state from the  $sd$ -shell because of its non-normal parity and small excitation energy. The nuclear deformation provides a simple mechanism for the existence of such a low-lying proton intruder state. The present study shows the importance of deformation for proton shell structure in neutron-rich nuclei and the change of the proton shell structure due to the excitation of one proton.

We would like to thank the RIKEN Ring Cyclotron staff members for their operation during the experiment. The present work was partially supported by the Grant-in-Aid for Scientific Research (No.15204018) by the Ministry of Education, Culture, Sports, Science and Technology, of Japan.

## References

- [1] D. Wilkinson, et al., Phys. Rev. 113 (1959) 563.
- [2] H. Iwasaki, et al., Phys. Lett. B 491 (2000) 8.
- [3] H. Iwasaki, et al., Phys. Lett. B 481 (2000) 7.

- [4] S. Shimoura, et al., Phys. Lett. B 560 (2003) 31.
- [5] S. Shimoura, et al., Phys. Lett. B 654 (2007) 87.
- [6] T. Suzuki, et al., Phys. Rev. C 67 (2003) 044302.
- [7] I. Hamamoto, Nucl. Phys. A 731 (2004) 211.
- [8] A. Bohr, B. R. Mottelson, Nuclear Structure, Vol. II, World Scientific (1998).
- [9] I. Hamamoto, S. Shimoura J. Phys. G 34 (2007) 2715
- [10] S. Michimasa, et al., Phys. Lett. B 638 (2006) 146.
- [11] H. Ryuto, et al., Nucl. Instr. and Meth. A 555 (2005) 1.
- [12] T. Kubo, et al., Nucl. Instr. and Meth. B 70 (1992) 309.
- [13] H. Kumagai, et al., Nucl. Instr. and Meth. A 470 (2001) 562.
- [14] S. Shimoura, Nucl. Instr. and Meth. A 525 (2004) 188.
- [15] M. Kurokawa, et al., IEEE TRANSACTIONS ON NUCLEAR SCIENCE 50 (2003) 1309.
- [16] S. Agostinelli, et al., Nucl. Instr. and Meth. A 506 (2003) 250.
- [17] Geant4 a toolkit for the simulation of the passage of particles through matter,  
<http://geant4.web.cern.ch/geant4/index.shtml>.
- [18] F. Ajzenberg-Selove, et al., Phys. Rev. C 17 (1978) 1283.
- [19] V. Guimarães, et al., Phys. Rev. C 61 (2000) 064609.
- [20] N. Aoi, et al., Phys. Rev. C 66 (2002) 014301.
- [21] R. Kalpakchieva, et al., Eur. Phys. J. A 7 (2000) 451.
- [22] P. D. Kunz, computer code DWUCK5, *unpublished*.
- [23] G. R. Satchler, Phys. Rev. C 55 (1997) 285.

- [24] C. J. Horowitz, Computational Nuclear Physics, Vol. I, Springer-Verlag (1991).
- [25] C. J. Horowitz, Nucl. Phys. A 368 (1981) 503.
- [26] A. Ingemarsson, et al., Nucl. Phys. A 676 (2000) 3.
- [27] A. Ingemarsson, et al., Nucl. Phys. A 696 (2001) 3.
- [28] B. A. Brown, A. Etchegoyen, W. D. M. Rae, The computer code OXBASH, MSU-NSCL report number 524 (1986).
- [29] T. Nagatomo, et al., Nucl. Phys. A 746 (2004) 509c
- [30] Y. Kanada-En'yo, et al., *submitted to* Phys. Rev C (arXiv:0706.3503v1 [nucl-th]).

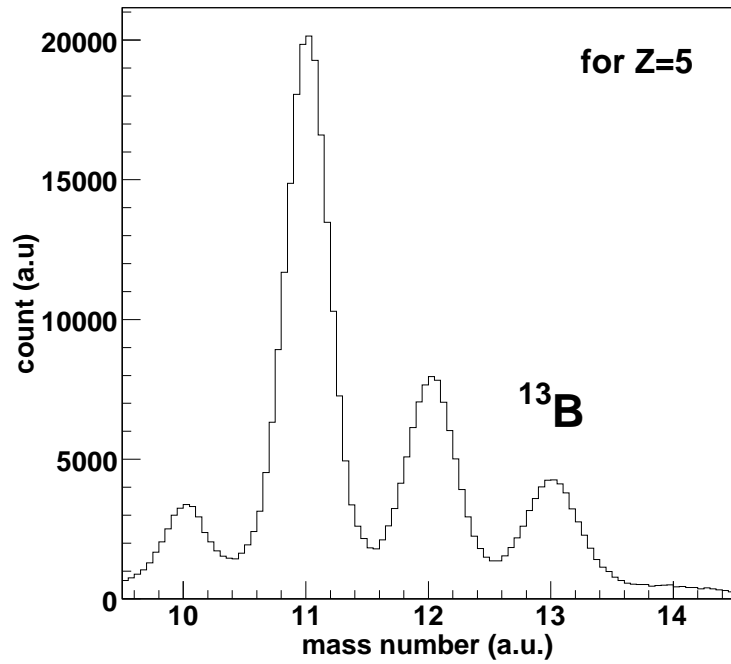


Fig. 1. Mass distribution of the outgoing particles for  $Z = 5$  extracted from the correlation between TOF and  $\Delta E$  measured with the plastic scintillator hodoscope.

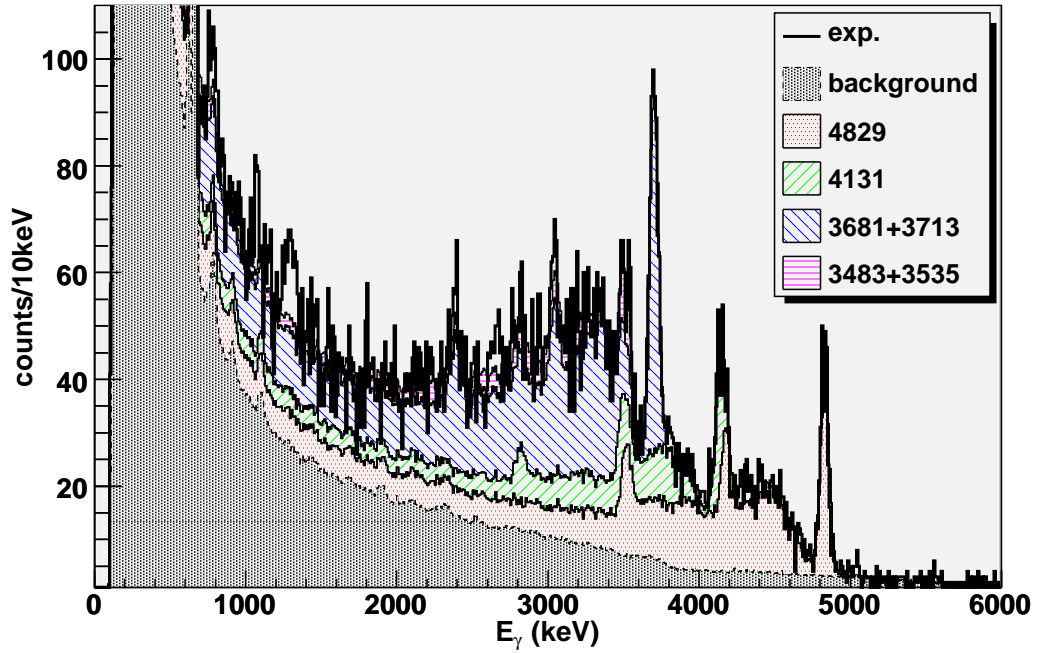


Fig. 2. Doppler corrected  $\gamma$ -ray spectrum in coincidence with  $^{13}\text{B}$  particles. The spectrum is decomposed with the sum of response functions of the GRAPE for the de-excitation and background  $\gamma$  rays. The resulting response functions are shown with hatched areas. The response functions for two doublets around 3.5 and 3.7 MeV are summed. The response function for the background includes the natural background and the decay of the  $^{12}\text{Be}$  isomer (see the text).

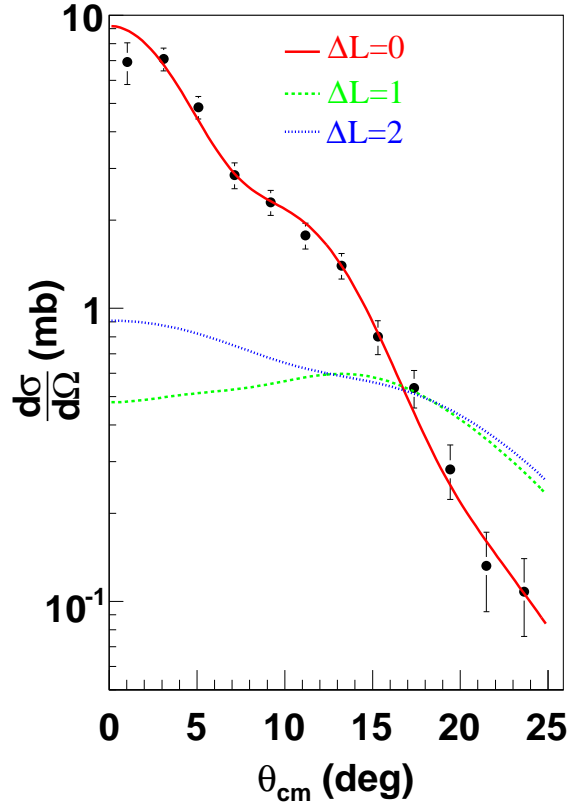


Fig. 3. Angular distribution of the 4.83-MeV excited  $^{13}\text{B}$ . Experimental data is shown by the filled circles with statistical errors. The solid, dotted and dashed curves show the DWBA predictions with assumptions of  $\Delta L = 0, 1,$  and  $2,$  respectively. See the text for more detail including the optical potentials.

Table 1

List of the relative populations of the excited states. The intensities are normalized by the most intense population. The errors are statistical only. In the last column, the spins and parities which have been assigned in the previous and present studies are listed. a: Present reaction of  ${}^4\text{He}({}^{12}\text{Be}, {}^{13}\text{B}\gamma)$ . b:  ${}^{11}\text{B}(\text{t}, \text{p}){}^{13}\text{B}$ . c:  ${}^9\text{Be}({}^{14}\text{B}, {}^{13}\text{B})\text{X}$ . d:  ${}^{14}\text{Be}$   $\beta$  delayed n. e:  ${}^{16}\text{O}({}^{14}\text{C}, {}^{17}\text{F}){}^{13}\text{B}$ . For the reaction b the relative intensity is at  $\theta_{\text{lab}} = 10^\circ$  and for the reaction e at  $\theta_{\text{c.m.}} = 5.4^\circ$ .

Relative intensities						
$E_x$ (MeV)	a	b	c	d	e	$J^\pi$
3.48	$0.19 \pm 0.05$	0.06	$0.60 \pm 0.14$			
3.53	$0.20 \pm 0.05$	0.19		1		
3.68	$0.74 \pm 0.07$	0.38	1			
3.71	$0.68 \pm 0.07$	0.25				
4.13	$0.49 \pm 0.04$	1	$0.04 \pm 0.04$			
4.83	1	0.03			1	$1/2^+$